Hindawi
Advances in High Energy Physics
Volume 2021, Article ID 9305605, 10 pages
https://doi.org/10.1155/2021/9305605

Research Article

Study of Production of (Anti-)deuteron Observed in Au+Au Collisions at $\sqrt{s_{\mathrm{NN}}} = 14.5$, 62.4, and 200 GeV

Ying Yuan [1,2]

[1]*Mathematics and Physics Teaching and Research Section, College of Pharmacy, Guangxi University of Chinese Medicine, Nanning 530200, China*
[2]*Guangxi Key Laboratory of Nuclear Physics and Nuclear Technology, Guangxi Normal University, Guilin 541004, China*

Correspondence should be addressed to Ying Yuan; wawayubao@qq.com

Received 18 June 2020; Revised 9 October 2020; Accepted 27 February 2021; Published 15 March 2021

Academic Editor: Bhartendu K. Singh

Transverse momentum distributions of deuterons and antideuterons in Au + Au collisions at $\sqrt{s_{\mathrm{NN}}} = 14.5$, 62.4, and 200 GeV with different centrality are studied in the framework of the multisource thermal model. Transverse momentum spectra are conformably and approximately described by the Tsallis distribution. The dependence of parameters (average transverse momenta, effective temperature, and entropy index) on event centrality is obtained. It is found that the parameters T increase and q decrease with increase of the average number of particles involved in collisions, which reveals the transverse excitation degree increases with collision centrality.

1. Introduction

The study of strongly interacting matter at extreme temperatures and densities is provided a chance by heavy ion collisions at ultrarelativistic energies [1–5]. The production mechanism of nuclei in ultrarelativistic heavy ion collisions deserves more investigation since it may give important message on the quantum chromodynamics (QCD) phase transition from quark-gluon plasma (QGP) to hadron gas (HG) [6, 7]. The RHIC is scheduled to run at the energies which are around the critical energy of phase transition from hadronic matter to QGP [8]. The theoretical study of nuclei and antinuclei has been undertaken for many years, for example, the thermal model and coalescence model [9–13]. In particular, the study of transport phenomena is major important to the understanding of many fundamental properties [14]. The spectra of transverse momentum of particles produced in high energy collisions are of high interest as soon as they provide us with an important information of the kinetic freeze-out state of the interacting system [15]. At the stage of kinetic freeze-out, the effective temperature is not a real temperature, and it describes the sum of excitation degree of the interacting system and the effect of transverse flow [16].

In this paper, using the Tsallis distribution [17–19] in the multisource thermal model to simulate the transverse momentum distributions of (anti-)deuterons in Au + Au collisions at RHIC, we compare them with experiment data taken from the STAR Collaboration [20]. The main purpose of this work is to extract the information on effective temperature, because it allows us to extract the kinetic freeze-out temperature.

2. The Model and Method

The model used in the present work is the multisource thermal model [21–23]. In this model, many emission sources are formed in high-energy nucleus-nucleus collisions. The different distributions can describe the emission sources and particle spectra, such as the Tsallis distribution, the standard (Boltzmann, Fermi-Dirac, and Bose-Einstein) distributions, the Tsallis+standard distributions [24–29], and the Erlang distribution [21]. The Tsallis distribution can be described by two or three standard distributions.

The experimental data of the transverse momentum spectrum of the particles are fitted by using the Tsallis distribution which can describe the temperature fluctuation in a

Table 1: Values of μ corresponding to the curves in Au + Au collisions at $\sqrt{s_{NN}} = 14.5$ GeV, $\sqrt{s_{NN}} = 62.4$ GeV, and $\sqrt{s_{NN}} = 200$ GeV for 0-10%, 10-20%, 20-40%, 40-60%, and 60-80% centralities.

$\sqrt{s_{NN}}$ (GeV)	Cross section	μ (MeV)
14.5	0-10%	288.9 ± 12.9
	10-20%	284.9 ± 12.9
	20-40%	278.7 ± 12.8
	40-60%	256.0 ± 12.4
	60-80%	227.3 ± 1.08
62.4	0-10%	66.1 ± 5.3
	10-20%	65.4 ± 5.2
	20-40%	60.7 ± 5.2
	40-60%	54.1 ± 5.2
	60-80%	44.6 ± 5.9
200	0-10%	28.4 ± 5.5
	10-20%	27.7 ± 5.1
	20-40%	27.4 ± 4.9
	40-60%	22.9 ± 4.9
	60-80%	18.2 ± 4.5

few sources to give an average value. The Tsallis distribution has many function forms [17–19, 24–31]. In the rest frame of a considered source, we choose a simplified form of the joint probability density function of transverse momentum (p_T) and rapidity (y) [8],

$$f(p_T, y) \propto \frac{d^2N}{dy dp_T} = \frac{gV}{(2\pi)^2} p_T \sqrt{p_T^2 + m_0^2} \cosh y \times \left[1 + \frac{q-1}{T}\left(\sqrt{p_T^2 + m_0^2}\cosh y - \mu\right)\right]^{-q/(q-1)}. \quad (1)$$

Here, N is the particle number, g is the degeneracy factor, V is the volume of emission sources, m_0 is the rest mass of the studied particle, T is the temperature which describes averagely a few sources (local equilibrium states), q is the entropy index which describes the degree of nonequilibrium among different states, and μ is the chemical potential which is related to $\sqrt{s_{NN}}$ [32]. In the RHIC energy region, the values of μ are shown in Table 1 [33]. We can extract the values of T, q, and V from reproducing the particle spectra, where T and q are fitted independently for the studied particle and V is related to other parameters.

The Monte Carlo distribution generating method is used to obtain p_T. Let r_1 denote the random numbers distributed uniformly in [0, 1]. A series of values of p_T can be obtained by

$$\int_0^{p_T} f_{p_T}(p_T) dp_T < r_1 < \int_0^{p_T + dp_T} f_{p_T}(p_T) dp_T. \quad (2)$$

Here, f_{p_T} is the transverse momentum probability density function which is an alternative representation of the Tsallis distribution as follows:

$$f_{P_T}(p_T) = \frac{1}{N}\frac{dN}{dp_T} = \int_{y_{min}}^{y_{max}} f(p_T, y) dy, \quad (3)$$

where y_{max} and y_{min} are the maximum and minimum rapidity, respectively.

Under the assumption of isotropic emission in the source rest frame, we use the Monte Carlo method to acquire the polar angle:

$$\theta = 2 \arcsin \sqrt{r_2}. \quad (4)$$

Here, r_2 denotes the random numbers distributed uniformly in [0, 1]. Thus, we can obtain a series of values of momentum and energy due to the momentum $p = p_T/\sin\theta$ and the energy $E = \sqrt{p^2 + m_0^2}$. Therefore, the corresponding values of rapidity can be obtained according to the definition of rapidity.

3. Results and Discussion

3.1. Transverse Momentum Spectra. Figure 1 demonstrates midrapidity ($|y| < 0.3$) transverse momentum spectra for deuterons in Au + Au collisions at $\sqrt{s_{NN}} = 14.5$ GeV for 0-10%, 10-20%, 20-40%, 40-60%, and 60-80% centralities. The symbols represent the experimental data of STAR Collaboration [20]. The solid lines are our calculated results fitted by using the Tsallis distribution based on eq. (1) in the region of midrapidity. The values of the related parameters T and q are given in Table 2 along with the χ^2/dof (χ^2 and number of degree of freedom). It is found that the calculations of the Tsallis distribution are in keeping with the experimental data well.

In Figures 2 and 3, the curves and symbols are similar to Figure 1. Figure 2 demonstrates midrapidity ($|y| < 0.3$) transverse momentum spectra for deuterons in Au + Au collisions at $\sqrt{s_{NN}} = 200$ GeV for 0-10%, 10-20%, 20-40%, 40-60%, and 60-80% centralities. The values of the related parameters T and q are given in Tables 3 and 4 along with the χ^2/dof. It is found that the calculations of the Tsallis distribution are in keeping with the experimental data well.

In Figures 4–6 demonstrates midrapidity ($|y| < 0.3$) transverse momentum spectra for antideuterons in Au + Au collisions at $\sqrt{s_{NN}} = 14.5$, 62.4, and 200 GeV for 0-10%, 10-20%, 20-40%, 40-60%, and 60-80% centralities. The curves and symbols are similar to Figure 1. One can see that the calculations also can describe approximately the experimental data of antideuterons with different centrality intervals of event. The values of the related parameters T and q are given in Tables 2–4.

3.2. Average Transverse Momenta. Figure 7 presents the centrality dependence of deuterons and antideuterons average transverse momenta ($\langle p_T \rangle$) at the midrapidity ($|y| < 0.3$) for $\sqrt{s_{NN}} = 14.5$, 62.4, and 200 GeV. The hollow symbols are the experiment data taken from the Figures 1–6, and the solid

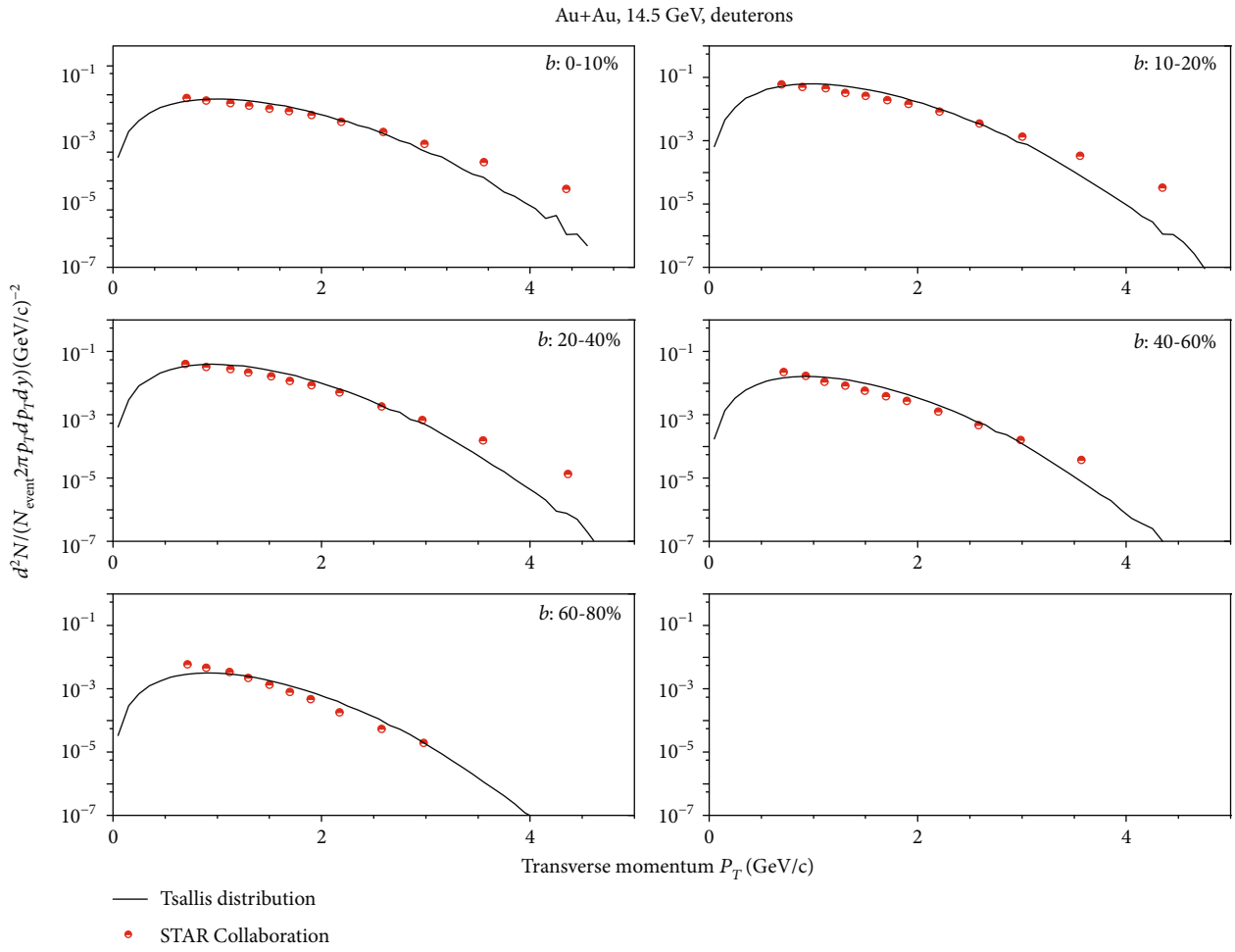

FIGURE 1: Deuteron transverse momentum spectra in Au + Au collisions at $\sqrt{s_{NN}}$ = 14.5 GeV for 0-10%, 10-20%, 20-40%, 40-60%, and 60-80% centralities. Calculations are shown by the solid lines. Experimental data taken from the STAR Collaboration [20] are represented by the symbols.

TABLE 2: Values of T, q, and χ^2/dof corresponding to the curves in Au + Au collisions at $\sqrt{s_{NN}}$ = 14.5 GeV for 0-10%, 10-20%, 20-40%, 40-60%, and 60-80% centralities. The "Ratios" is the average ratios of experimental data to model.

Figure	Type 1	Type 2	T (GeV)	q	χ^2/dof	Ratios
Figure 1	d	0-10%	0.507 ± 0.002	1.125 ± 0.017	0.055	0.805
		10-20%	0.487 ± 0.011	1.145 ± 0.166	0.053	0.742
		20-40%	0.467 ± 0.054	1.165 ± 0.084	0.119	0.788
		40-60%	0.427 ± 0.008	1.185 ± 0.045	0.150	0.848
		60-80%	0.407 ± 0.001	1.205 ± 0.007	0.639	1.191
Figure 4	$\bar{d}$	0-10%	0.507 ± 0.001	1.105 ± 0.001	0.564	0.884
		10-20%	0.487 ± 0.001	1.125 ± 0.001	0.239	1.005
		20-40%	0.447 ± 0.001	1.145 ± 0.001	0.331	0.939
		40-60%	0.387 ± 0.001	1.165 ± 0.001	0.619	0.914
		60-80%	0.347 ± 0.001	1.185 ± 0.001	1.508	0.960

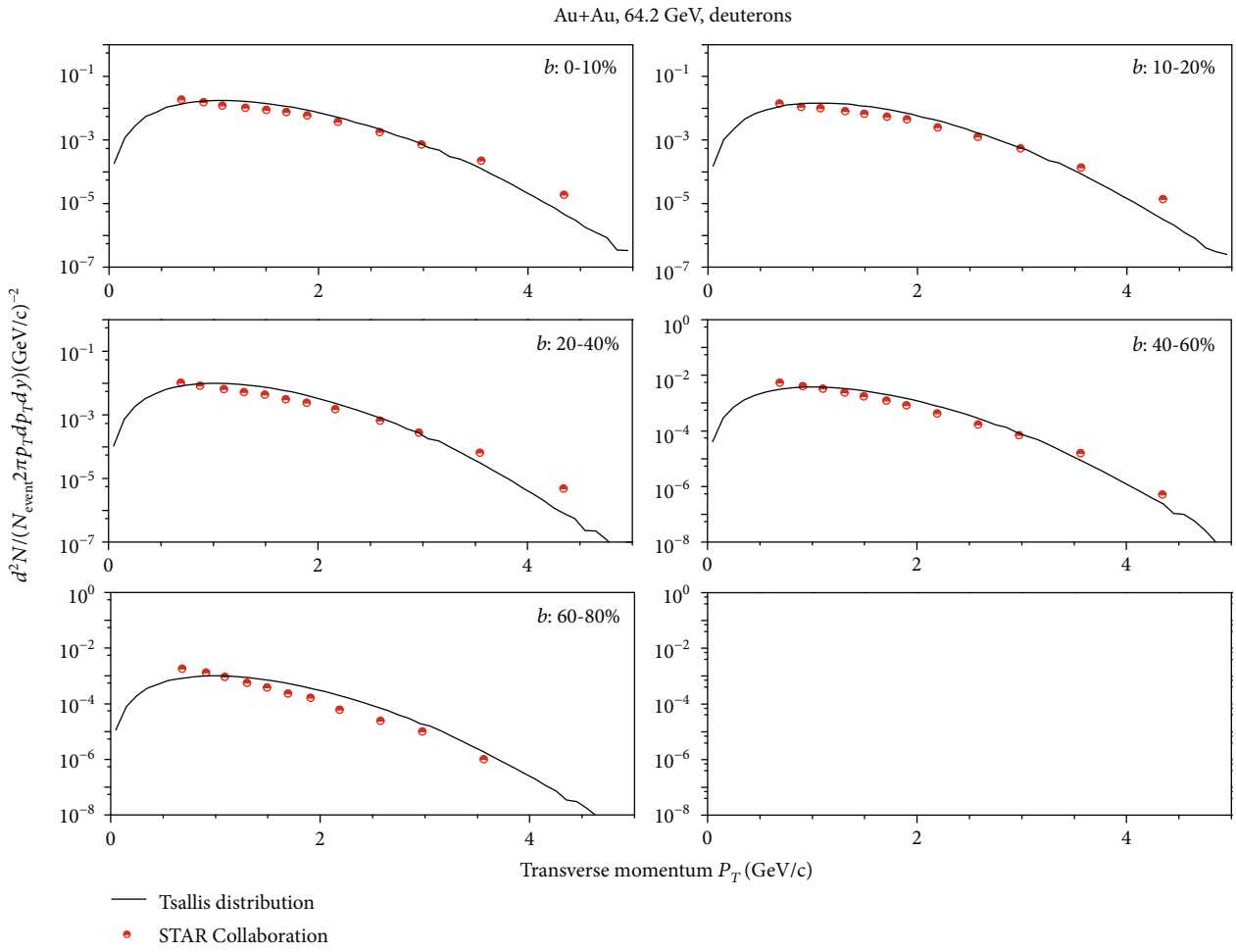

FIGURE 2: Deuteron transverse momentum spectra in Au + Au collisions at $\sqrt{s_{NN}} = 62.4$ GeV for 0-10%, 10-20%, 20-40%, 40-60%, and 60-80% centralities. Calculations are shown by the solid lines. Experimental data taken from the STAR Collaboration [20] are represented by the symbols.

symbols are the calculations of the Tsallis distribution. The calculations can be obtained by

$$\langle p_T \rangle = \frac{\sum p_{T1}\alpha}{\sum \alpha}. \quad (5)$$

Here, p_{T1} is the value of transverse momentum corresponding to the experimental data, and α is the value of $d^2N/N_{event}2\pi p_T dp_T dy$ that corresponds to the p_{T1}.In this figure, one sees that the calculations can describe the experimental data well in the range of the errors permitted. For deuterons, the values of average transverse momenta in the different incident energy get closer with decrease of centrality percentage. It has indicated that the transverse excitation degree increases with collision centrality.

3.3. Dependence of Parameters on Number of Participating Nucleons. Figures 8 and 9 give the change trends of parameters (T and q) with the average number of participants for deuterons and antideuterons produced in Au + Au collision at the midrapidity ($|y| < 0.3$) for $\sqrt{s_{NN}} = 14.5$, 62.4, and 200 GeV. The symbols represent the parameter values extracted from Figures 1–6 and listed in Tables 2–4.

From Figures 8 and 9, we can see that the values of T parameters increase with decrease of centrality percentage, and the values of q parameters increase with increase of centrality percentage. Entropy is a physical quantity that represents the degree of chaos in the system. When a central collision occurs, the motion law of the final state particles is complex, and the whole system is in a higher state of order, so the entropy value is small. In the central region where the collision occurs, with the increase of the intensity of the collision, the corresponding effective temperature increases. The dependence of effective temperature on collision energy increases with the increase of collision energy. Under the same collision parameters, the entropy increases with the increase of collision energy, indicating that the higher the collision energy is, the more different microscopic states the particle may have, and the more disordered the system becomes. The kinetic freeze-out temperature can be extracted

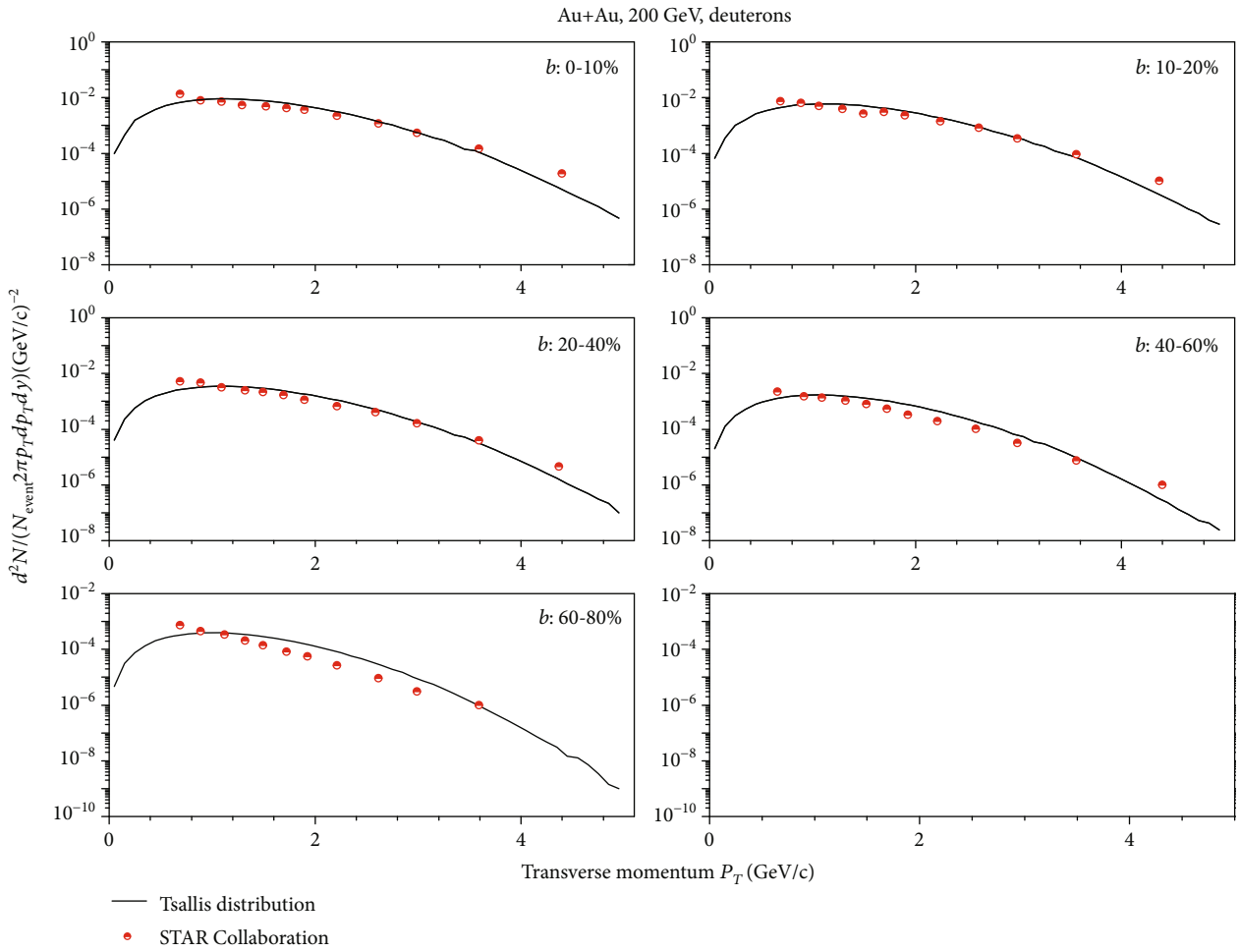

FIGURE 3: Deuteron transverse momentum spectra in Au + Au collisions at $\sqrt{s_{NN}}$ = 200 GeV for 0-10%, 10-20%, 20-40%, 40-60%, and 60-80% centralities. Calculations are shown by the solid lines. Experimental data taken from the STAR Collaboration [20] are represented by the symbols.

TABLE 3: Values of T, q, and χ^2/dof corresponding to the curves in Au + Au collisions at $\sqrt{s_{NN}}$ = 62.4 GeV for 0-10%, 10-20%, 20-40%, 40-60%, and 60-80% centralities. The "Ratios" is the average ratios of experimental data to model.

Figure	Type 1	Type 2	T (GeV)	q	χ^2/dof	Ratios
Figure 2	d	0-10%	0.607 ± 0.008	1.135 ± 0.051	0.037	0.785
		10-20%	0.587 ± 0.004	1.155 ± 0.038	0.061	0.711
		20-40%	0.527 ± 0.006	1.175 ± 0.022	0.124	0.731
		40-60%	0.507 ± 0.003	1.195 ± 0.010	0.107	0.887
		60-80%	0.487 ± 0.001	1.215 ± 0.003	0.274	0.910
Figure 5	$\bar{d}$	0-10%	0.607 ± 0.001	1.135 ± 0.005	2.527	0.712
		10-20%	0.567 ± 0.001	1.155 ± 0.005	1.464	0.834
		20-40%	0.527 ± 0.001	1.175 ± 0.003	2.231	0.833
		40-60%	0.507 ± 0.001	1.195 ± 0.003	2.099	1.095
		60-80%	0.407 ± 0.002	1.215 ± 0.001	3.303	0.966

Table 4: Values of T, q, and χ^2/dof corresponding to the curves in Au + Au collisions at $\sqrt{s_{NN}} = 200$ GeV for 0-10%, 10-20%, 20-40%, 40-60%, and 60-80% centralities. The "Ratios" is the average ratios of experimental data to model.

Figure	Type 1	Type 2	T (GeV)	q	χ^2/dof	Ratios
Figure 3	d	0-10%	0.667 ± 0.004	1.145 ± 0.021	0.069	0.889
		10-20%	0.647 ± 0.004	1.175 ± 0.017	0.040	0.847
		20-40%	0.627 ± 0.008	1.195 ± 0.036	0.004	0.989
		40-60%	0.567 ± 0.001	1.215 ± 0.006	0.048	0.782
		60-80%	0.507 ± 0.001	1.235 ± 0.003	0.063	0.906
Figure 6	$\bar{d}$	0-10%	0.667 ± 0.001	1.145 ± 0.005	0.086	0.795
		10-20%	0.647 ± 0.001	1.165 ± 0.005	0.047	0.770
		20-40%	0.627 ± 0.001	1.195 ± 0.004	0.048	0.802
		40-60%	0.607 ± 0.001	1.215 ± 0.002	0.055	0.853
		60-80%	0.597 ± 0.001	1.255 ± 0.001	0.206	1.183

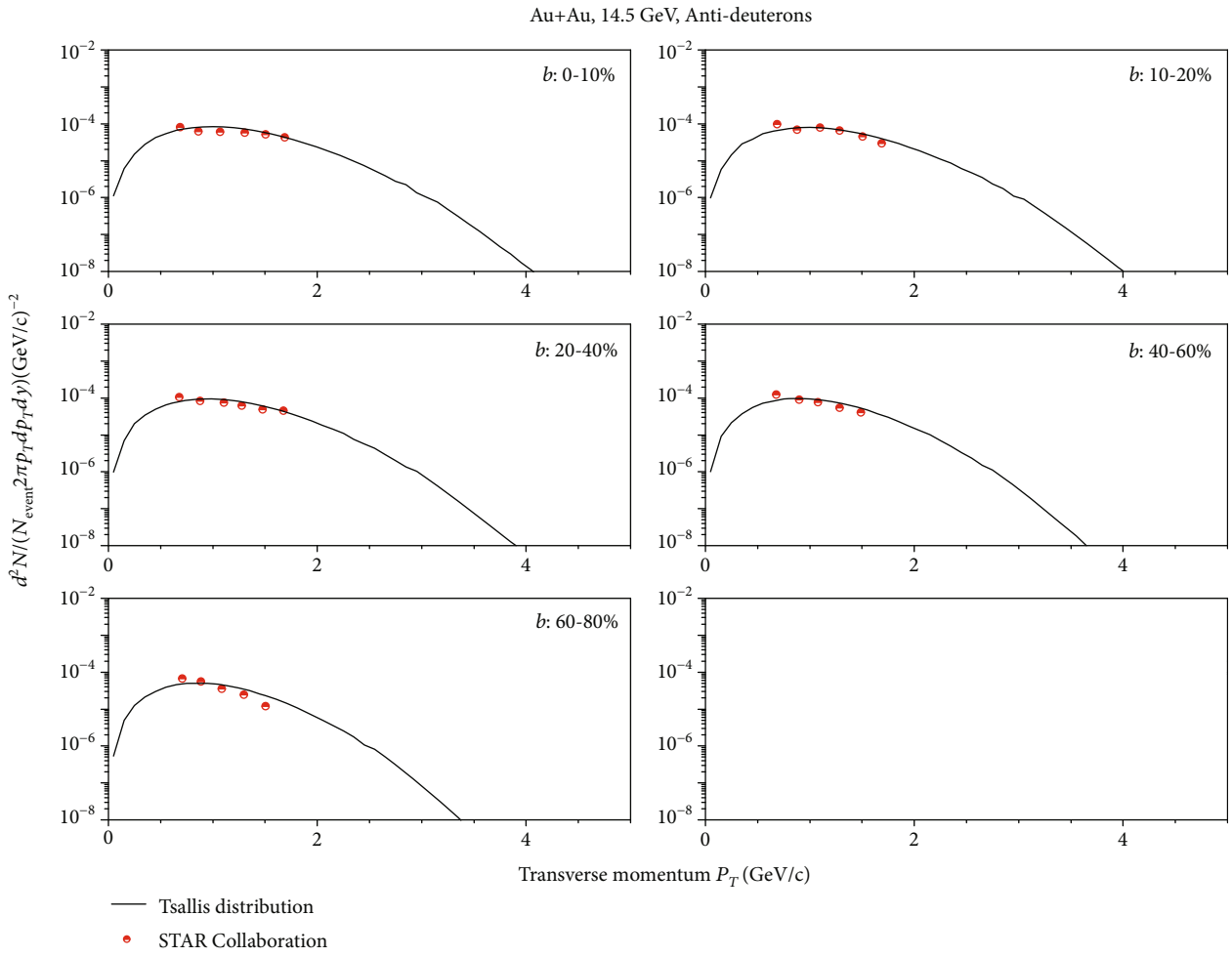

Figure 4: Antideuteron transverse momentum spectra in Au + Au collisions at $\sqrt{s_{NN}} = 14.5$ GeV for 0-10%, 10-20%, 20-40%, 40-60%, and 60-80% centralities. Calculations are shown by the solid lines. Experimental data taken from the STAR Collaboration [20] are represented by the symbols.

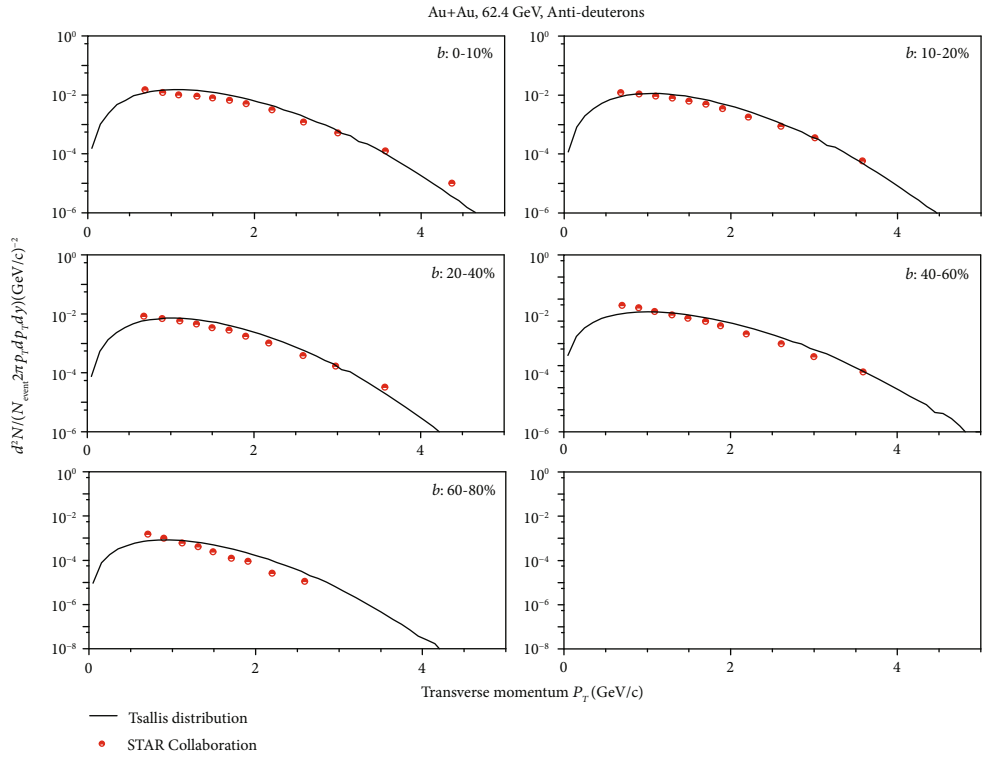

Figure 5: Antideuteron transverse momentum spectra in Au + Au collisions at $\sqrt{s_{NN}} = 62.4$ GeV for 0-10%, 10-20%, 20-40%, 40-60%, and 60-80% centralities. Calculations are shown by the solid lines. Experimental data taken from the STAR Collaboration [20] are represented by the symbols.

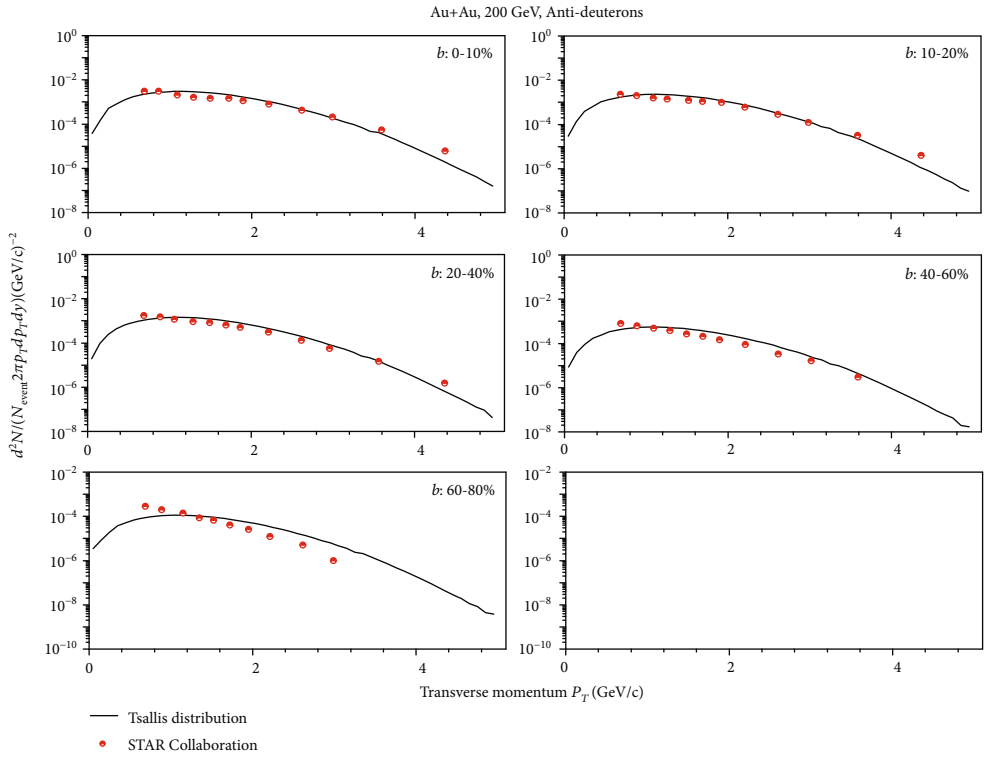

Figure 6: Antideuteron transverse momentum spectra in Au + Au collisions at $\sqrt{s_{NN}} = 200$ GeV for 0-10%, 10-20%, 20-40%, 40-60%, and 60-80% centralities. Calculations are shown by the solid lines. Experimental data taken from the STAR Collaboration [20] are represented by the symbols.

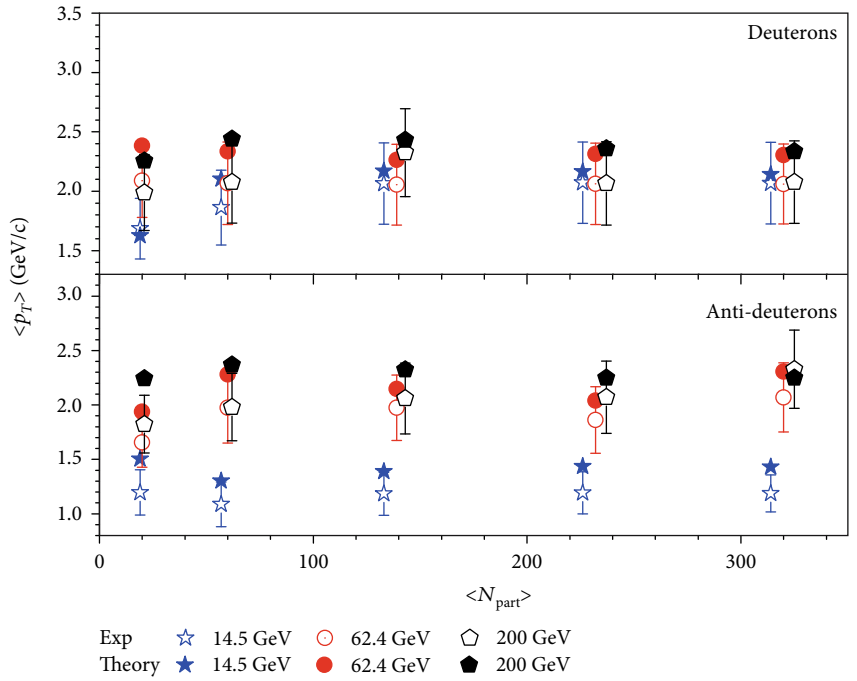

FIGURE 7: Deuterons and antideuterons average transverse momenta ($\langle p_T \rangle$) as a function of ($\langle N_{part} \rangle$) at midrapidity ($|y| < 0.3$) for $\sqrt{s_{NN}}$ = 14.5, 62.4, and 200 GeV. Calculations are shown by the solid symbols. Experimental data taken from the Figures 1–6 are represented by the hollow symbols.

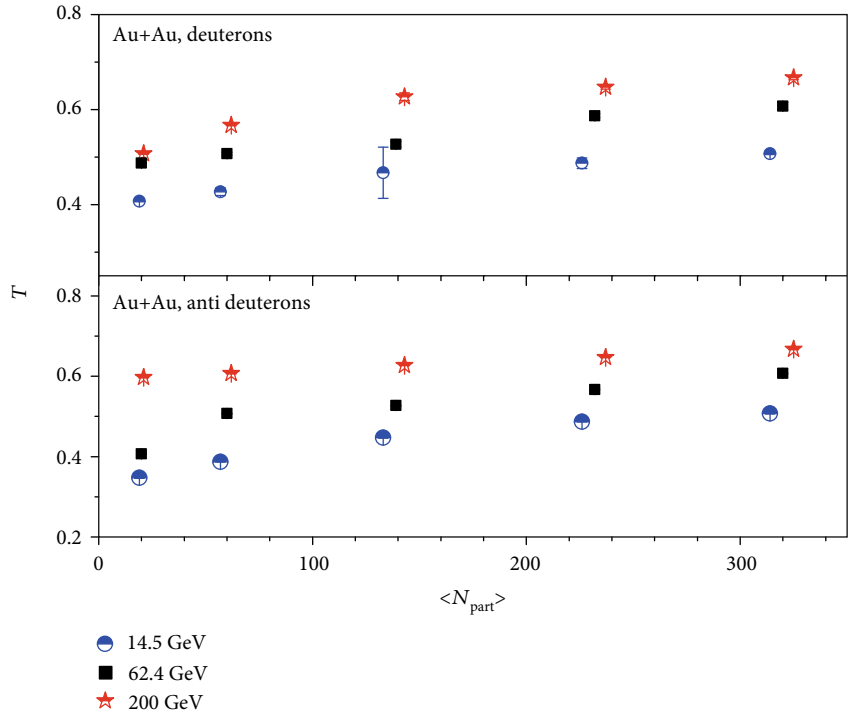

FIGURE 8: Dependence of T on the average number of participants for deuterons and antideuterons in events with different centrality intervals. The symbols represent the parameter values listed in Tables 2–4.

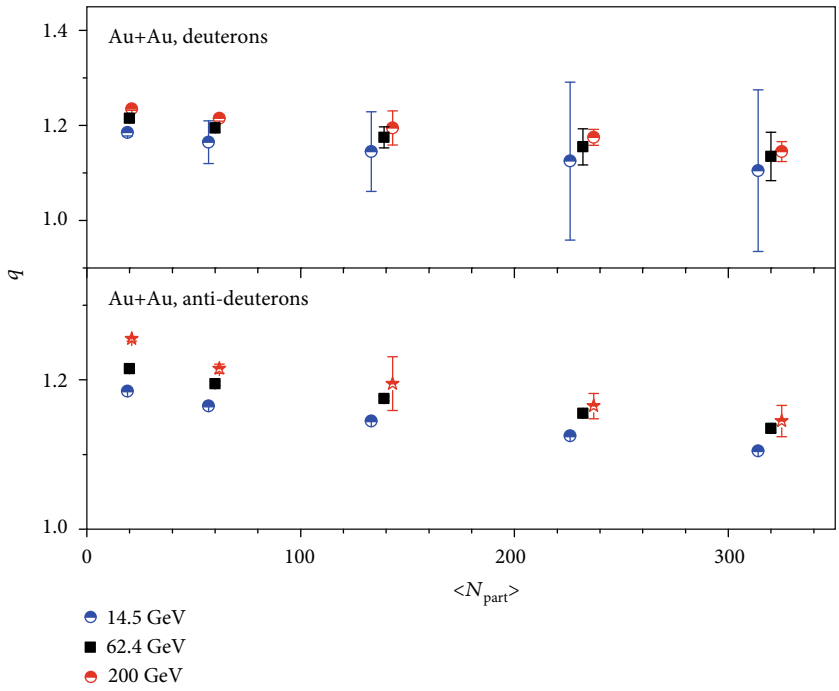

FIGURE 9: Dependence of q on the average number of participants for deuterons and antideuterons in events with different centrality intervals. The symbols represent the parameter values listed in Tables 2–4.

from the effective temperature; the correlation between Kinetic freeze-out temperature and centrality will be focused in the future work.

4. Summary and Outlook

In summary, we have presented the transverse momentum distributions of (anti-)deuterons in Au + Au collisions at $\sqrt{s_{\mathrm{NN}}} = 14.5$, 62.4, and 200 GeV for 0-10%, 10-20%, 20-40%, 40-60%, and 60-80% centralities. The Tsallis distribution in the multisource thermal model has been used in all calculations. Based on this model, we have investigated transverse momentum distributions of (anti-)deuterons and the law about effective temperature and entropy with the centrality of collision. In conclusion, it can give the agreement between calculation results and the experimental data. The effective temperature extracted from d and $\bar{d}$ increases with decrease of centrality percentage at the same incident energy, and the entropy index decreases with decrease of centrality percentage at the same incident energy. And at the same collision centrality, they increase with increase of incident energy. But the Kinetic freeze-out temperature and the evolution of time during the collision have yet to be studied in depth.

Data Availability

The data used to support the findings of this study are included within the article and are cited at relevant places within the text as references.

Conflicts of Interest

The author declares that there is no conflict of interests regarding the publication of this paper.

Acknowledgments

This work was supported by the Introduction of Doctoral Starting Funds of Scientific Research of Guangxi University of Chinese Medicine under Grant No. 2018BS024, the Natural Science Foundation of Guangxi Zhuangzu Autonomous Region of China under Grant no. 2012GXNSFBA053011, the Research support project of Guangxi institutions of higher learning (No. 200103YB071), and the Open Project of Guangxi Key Laboratory of Nuclear Physics and Nuclear Technology (No. NLK2020-03).

References

[1] C. Alt, T. Anticic, B. Baatar et al., "Energy dependence of Λ and Ξ production in central Pb+Pb collisions at 20A, 30A, 40A, 80A, and 158A GeV measured at the CERN Super Proton Synchrotron," *Physical Review C*, vol. 78, no. 3, article 034918, 2008.

[2] J. X. Sun, F. H. Liu, and E. Q. Wang, "Pseudorapidity distributions of charged particles and contributions of leading nucleons in Cu-Cu collisions at high energies," *Chinese Physics Letters*, vol. 27, no. 3, article 032503, 2010.

[3] E. Q. Wang, F. H. Liu, M. A. Rahim, S. Fakhraddin, and J. X. Sun, "Singly and doubly charged projectile fragments in nucleus-emulsion collisions at Dubna energy in the framework of the multi-source model," *Chinese Physics Letters*, vol. 28, no. 8, article 082501, 2011.

[4] B. C. Li and M. Huang, "Strongly coupled matter near phase transition," *Journal of Physics G: Nuclear and Particle Physics*, vol. 36, no. 6, article 064062, 2009.

[5] F. H. Liu, "Anisotropic emission of charged mesons and structure characteristic of emission source in heavy ion collisions at 1–2A GeV," *Chinese Physics B*, vol. 17, no. 8, pp. 883–895, 2008.

[6] R. Arsenescu, C. Baglin, H. P. Beck et al., "An investigation of the antinuclei and nuclei production mechanism in Pb + Pb collisions at 158 A GeV," *New Journal of Physics*, vol. 5, p. 150, 2003.

[7] Q. F. Li, Y. J. Wang, X. B. Wang, and C. W. Shen, "Helium-3 production from Pb+Pb collisions at SPS energies with the UrQMD model and the traditional coalescence afterburner," *Science China: Physics, Mechanics and Astronomy*, vol. 59, no. 3, article 632002, 2016.

[8] H.-L. Lao, H.-R. Wei, F.-H. Liu, and R. A. Lacey, "An evidence of mass-dependent differential kinetic freeze-out scenario observed in Pb-Pb collisions at 2.76 TeV," *The European Physical Journal A*, vol. 52, no. 7, p. 203, 2016.

[9] S. Mrówczyński and P. Słoń, "Hadron-deuteron correlations and production of light nuclei in relativistic heavy-ion collisions," *Acta Physica Polonica B*, vol. 51, no. 8, article 1739, 2020.

[10] S. Mrowczynski, "Production of light nuclei in the thermal and coalescence models," *Acta Physica Polonica B*, vol. 48, no. 4, pp. 707–716, 2017.

[11] S. Bazak and S. Mrówczyński, "^{4}He versus ^{4}Li and production of light nuclei in relativistic heavy-ion collisions," *Modern Physics Letters A*, vol. 33, no. 25, article 1850142, 2018.

[12] P. Liu, J. H. Chen, Y. G. Ma, and S. Zhang, "Production of light nuclei and hypernuclei at High Intensity Accelerator Facility energy region," *Nuclear Science and Techniques*, vol. 28, no. 4, p. 55, 2017.

[13] F. X. Liu, G. Chen, Z. L. Zhe, D. M. Zhou, and Y. L. Xie, "Light (anti) nuclei production in Cu+Cu collisions at $\sqrt{s_{NN}}$ =200 GeV," *The European Physical Journal A*, vol. 55, p. 160, 2019.

[14] B. C. Li, Y. Y. Fu, L. L. Wang, and F. H. Liu, "Dependence of elliptic flows on transverse momentum and number of participants in Au+Au collisions at $\sqrt{s_{NN}}$ = 200 GeV," *Journal of Physics G: Nuclear and Particle Physics*, vol. 40, no. 2, article 025104, 2013.

[15] Y. H. Chen, F. H. Liu, and E. K. Sarkisyan-Grinbaum, "Event patterns from negative pion spectra in proton-proton and nucleus-nucleus collisions at SPS," *Chinese Physics C*, vol. 42, no. 10, article 104102, 2018.

[16] M. Waqas, F. H. Liu, L. L. Li, and H. M. Alfanda, "Analysis of effective temperature and kinetic freeze-out volume in high energy nucleus-nucleus and proton-proton collisions," 2020, http://arxiv.org/abs/hep-ph/2001.06796v1.

[17] C. Tsallis, "Possible generalization of Boltzmann-Gibbs statistics," *Journal of Statistical Physics*, vol. 52, no. 1-2, pp. 479–487, 1988.

[18] T. S. Biró, G. Purcsel, and K. Ürmössy, "Non-extensive approach to quark matter," *The European Physical Journal A*, vol. 40, no. 3, p. 325, 2009.

[19] J. Cleymans and D. Worku, "Relativistic thermodynamics: transverse momentum distributions in high-energy physics," *The European Physical Journal A*, vol. 48, no. 11, p. 160, 2012.

[20] STAR Collaboration, "Beam energy dependengce of (anti-)deuteron production in Au+Au collisions at RHIC," *Physical Review C*, vol. 99, no. 6, article 064905, 2019.

[21] F. H. Liu, Y. Q. Gao, and H. R. Wei, "On descriptions of particle transverse momentum spectra in high energy collisions," *Advances in High Energy Physics*, vol. 2014, Article ID 293873, 12 pages, 2014.

[22] F. H. Liu, Y. Q. Gao, T. Tian, and B. C. Li, "Unified description of transverse momentum spectrums contributed by soft and hard processes in high-energy nuclear collisions," *European Physical Journal A*, vol. 50, no. 6, p. 94, 2014.

[23] F. H. Liu and J. S. Li, "Isotopic production cross section of fragments in ^{56}Fe +p and ^{136}Xe (^{124}Xe)+Pb reactions over an energy range from 300 A to 1500 A MeV," *Physical Review C*, vol. 78, no. 4, article 044602, 2008.

[24] F. Büyükkiliç and D. Demirhan, "A fractal approach to entropy and distribution functions," *Physics Letters A*, vol. 181, no. 1, pp. 24–28, 1993.

[25] J. Chen, Z. Zhang, G. Su, L. Chen, and Y. Shu, "q-generalized Bose-Einstein condensation based on Tsallis entropy," *Physics Letters A*, vol. 300, no. 1, pp. 65–70, 2002.

[26] J. M. Conroy and H. G. Miller, "Color superconductivity and Tsallis statistics," *Physical Review D*, vol. 78, no. 5, article 054010, 2008.

[27] F. Pennini, A. Plastino, and A. R. Plastino, "Tsallis entropy and quantal distribution functions," *Physics Letters A*, vol. 208, no. 4-6, pp. 309–314, 1995.

[28] A. M. Teweldeberhan, A. R. Plastino, and H. G. Miller, "On the cut-off prescriptions associated with power-law generalized thermostatistics," *Physics Letters A*, vol. 343, no. 1-3, pp. 71–78, 2005.

[29] J. M. Conroy, H. G. Miller, and A. R. Plastino, "Thermodynamic consistency of the _q_ -deformed Fermi-Dirac distribution in nonextensive thermostatics," *Physics Letters A*, vol. 374, no. 45, pp. 4581–4584, 2010.

[30] H. Zheng and L. Zhu, "Comparing the Tsallis distribution with and without thermodynamical description in collisions," *Advances in High Energy Physics*, vol. 2016, Article ID 9632126, 10 pages, 2016.

[31] H. Zheng and L. Zhu, "Can Tsallis distribution fit all the particle spectra produced at RHIC and LHC?," *Advances in High Energy Physics*, vol. 2015, Article ID 180491, 9 pages, 2015.

[32] A. Andronic, P. Braun-Munzinger, and J. Stachel, "The horn, the hadron mass spectrum and the QCD phase diagram - the statistical model of hadron production in central nucleus-nucleus collisions," *Nuclear Physics A*, vol. 834, no. 1-4, pp. 237c–240c, 2010.

[33] STAR Collaboration, "Bulk properties of the medium produced in relativistic heavy-ion collisions from the Beam Energy Scan Program," *Physical Review C*, vol. 96, no. 4, article 044904, 2017.